Article

Spatial Concentration Profiles for the Catalytic Partial Oxidation of Jet Fuel Surrogates in a Rh/Al$_2$O$_3$ Coated Monolith

Julian N. Bär [1], Claudia Antinori [2], Lubow Maier [2] and Olaf Deutschmann [1,2,*]

[1] Institute for Chemical Technology and Polymer Chemistry at Karlsruhe Institute of Technology (KIT), 76131 Karlsruhe, Germany; julian.baer@kit.edu

[2] Institute of Catalysis Research and Technology at Karlsruhe Institute of Technology (KIT), 76131 Karlsruhe, Germany; claudia.antinori@kit.edu (C.A.); lubow.maier@kit.edu (L.M.)

* Correspondence: deutschmann@kit.edu; Tel.: +49-721-608-43064

Abstract: The catalytic partial oxidation (CPOX) of several hydrocarbon mixtures, containing *n*-dodecane (DD), 1,2,4-trimethylbenzene (TMB), and benzothiophene (BT) as a sulfur compound was studied over a Rh/Al$_2$O$_3$ honeycomb catalyst. The in-situ sampling technique SpaciPro was used in this study to investigate the complex reaction system which consisted of total and partial oxidation, steam reforming, and the water gas shift reaction. The mixtures of 83 vol % DD, 17 vol % TMB with and without addition of the sulfur compound BT, as well as the pure hydrocarbons were studied at a molar C/O-ratio of 0.75. The spatially resolved concentration and temperature profiles inside a central channel of the catalyst revealed three reaction zones: an oxidation zone, an oxy-reforming zone, and a reforming zone. Hydrogen formation starts in the oxy-reforming zone, not directly at the catalyst inlet, contrary to methane CPOX on Rh. In the reforming zone, in which steam reforming is the predominant reaction, even small amounts of sulfur (10 mg S in 1 kg fuel) block active sites.

Keywords: in-situ sampling; spatial profiles; hydrogen generation; jet fuel; sulfur; rhodium

1. Introduction

The catalytic partial oxidation (CPOX) of liquid hydrocarbons over rhodium at short contact times is an efficient route to on-board syngas production for a fuel cell with the reformer and the fuel cell forming an auxiliary power unit [1–6]. Rh/Al$_2$O$_3$ catalysts are the most efficient catalysts for a high syngas yield [7–15]. In-situ investigations on the CPOX of methane as well as microkinetic modeling studies were crucial to unravel possible reaction pathways in order to establish reaction mechanisms and to gain an insight into different reaction zones [10,12,15–18]. In these papers, it is reported that the CPOX process follows a reaction sequence, in which the reaction system could be divided into two reaction zones along the catalyst. In the first zone, methane is predominantly oxidized, either totally to CO$_2$ and H$_2$O, or accompanied by some formation of CO and H$_2$ via partial oxidation. Due to the highly exothermic total oxidation, a hot spot occurs in the first few millimeters of the catalyst. Within this oxy-reforming zone, oxygen is completely consumed. In the second reaction zone, the reforming zone, the formed water is consumed by endothermic steam reforming. The water gas shift reaction occurs and influences the ratio between H$_2$/H$_2$O and CO/CO$_2$. The chemical kinetics of CPOX are thoroughly discussed in the literature [10,15,16,18–20]. As hydrogen is detected in the first reaction zone for methane CPOX on rhodium, a direct route for partial oxidation was suggested. However, the mass transport of oxygen is the limiting factor in this zone, leading to a strong radial gradient of the oxygen concentration inside the catalytic channel. Additionally, capillary-based in-situ techniques revealed further reaction pathways, e.g., the homogeneous dehydrogenation of

ethanol to formaldehyde for CPOX of ethanol [21]. The evolution of a detailed microkinetic reaction mechanism for the CPOX of higher hydrocarbons is challenging due to the occurrence of numerous catalytic reactions as well as homogeneous side reactions. Therefore, simplified models are used, e.g., Hartmann et al. [22] introduced two global reactions for the dissociative adsorption of the fuel (*i*-octane) and coupled these reactions with a detailed catalytic reaction mechanism for the catalytic partial oxidation of adsorbed C1–C3-species. Additionally, due to high temperatures, a detailed gas-phase mechanism with 857 gas-phase species along with 7193 irreversible reactions [23] had to be applied to predict the experimental observations.

Coking or catalyst poisoning affects the process during long-term operation. Nevertheless, a high syngas yield with low by-product formation and stable operation has been achieved for many different hydrocarbons and logistic fuels [1–5,24–34]. Still missing for sulfur-containing jet fuels are spatially-resolved concentration profiles, which are crucial for the understanding of the interplay between the main reactions and side reactions, e.g., cracking reactions, in dependence on the axial position. A realistic jet fuel, such as specifications of JP-8, JET A, and JET A1 [34], contains sulfur compounds, influencing activity and ageing of the catalyst.

In a recently published study, we investigated the CPOX of surrogates of jet fuels on Rh and observed an impact of sulfur on conversion and selectivity [34]. Only the CO/CO_2 ratio remained unaffected by the sulfur addition. To extend our previous study to a fundamental understanding of the position-dependent interplay of the occurring heterogeneous and homogeneous reactions, we focus herein on the in-situ investigation of the CPOX of these surrogates. The surrogates are composed of *n*-dodecane, 1,2,4-trimethylbenzene, and benzothiophene as a model sulfur compound. We collect spatially-resolved temperature and concentration profiles inside a channel of the honeycomb catalyst using SpaciPro, our previously described capillary-based sampling technique [18,21]. The principle of this technique is based on the collection of gas samples of the gas stream inside a monolithic channel of a honeycomb catalyst, analyzing its constituents using Fourier-transformed infrared and mass spectrometry.

2. Results and Discussion

2.1. Spatially-Resolved Concentration and Temperature Profiles

The catalytic partial oxidation of fuel blends, consisting of *n*-dodecane, 1,2,4-trimethylbenzene, and benzothiophene was investigated for a C/O-ratio of 0.75. For all investigations, a central channel was chosen for the collection of the concentration profiles. In all figures, the axial position $z = 0$ mm was defined as the start of the catalyst section.

The sulfur-free surrogate Su 17 is discussed as reference case (Figure 1). From $z = 0$ to 1.5 mm, the mole fraction of oxygen shows a steep decrease. Further downstream at the axial range of 1.5 mm $< z <$ 3 mm, oxygen is consumed at a lower rate, which is indicated by a smaller decline in the molar fraction in axial direction. Oxygen is completely consumed at the axial position of 3 mm inside the catalyst. A similar trend was observed for the molar fraction of the hydrocarbon fuel, as its slope shows a significant change at the position $z = 1.5$ mm. For $z > 1.5$ mm, the negative slope of the molar fraction of hydrocarbons along the axial coordinate decreases. At the position $z = 1.25$ mm (H_2O) and $z = 1.5$ mm (CO_2), the molar fractions of H_2O and CO_2 show a maximum after a steep increase starting at $z = 0$. However, for $z > 1.5$ mm, the molar fraction of CO_2 stays constant at $x_{CO_2} = 0.019$. After reaching its maximum at a molar fraction of $x_{H_2O} = 0.029$ ($z = 1.25$), water is consumed again, resulting in a decrease in molar fraction to $x_{H_2O} = 0.013$ ($z = 10$ mm). The formation of hydrogen starts at the axial position of 1.25 mm, with a steady increase over the length of the catalyst to a molar fraction of $x_{H_2} = 0.034$ ($z = 10$ mm). Downstream of the region $z = 0$–0.5 mm, in which the molar fraction of CO shows a sharp increase, a decrease to a local minimum of $x_{CO} = 0.004$ at the position $z = 1$ mm is reproducibly observed. Further downstream, CO is generated in the reforming zone ($z > 3$ mm) in the absence of oxygen. A maximum value of $x_{CO} = 0.027$ is reached at the catalyst outlet.
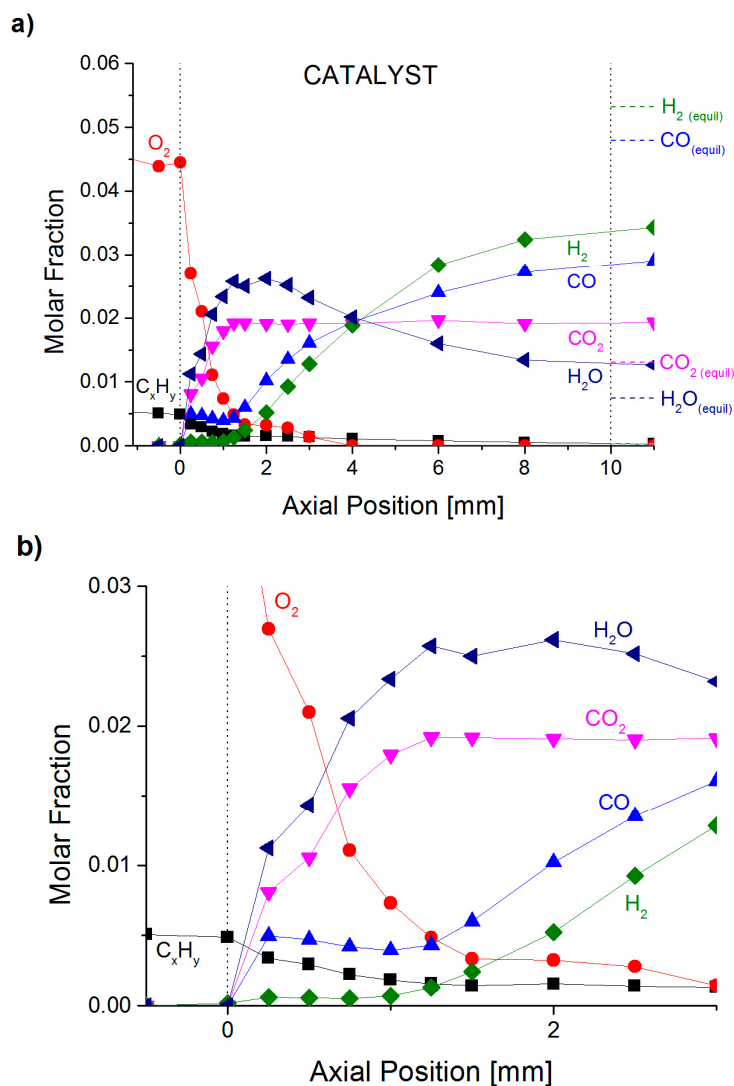
a)

b)

Figure 1. (**a**) Molar fraction of reactants and products as function of the axial coordinate z for the catalytic partial oxidation (CPOX) of the fuel "Su 17". Su 17 contains 83 vol % *n*-dodecane and 17 vol % 1,2,4-trimethylbenzene. The axial section of -1 mm $< z <$ 11 mm is chosen in order to improve the visibility of the molar fractions inside the catalyst ($z = 0$–10 mm). Dashed lines represent thermodynamic equilibrium values; (**b**) zoomed version of (**a**) within the oxidation zone and the oxy-reforming zone (-0.5 mm $< z <$ 3 mm).

The gas-phase and wall temperature profiles, which were collected by means of a thermocouple and an optical fiber, respectively, are shown in Figure 2 for Su 17. Due to the highly exothermic total oxidation, which predominantly occurs within the first 1.5 mm in the oxidation zone, a hot spot occurs on the surface (T_{wall} = 725 °C) at z = 2 mm and at z = 2.5 mm in the gas phase (T_{gas} = 715 °C). In the last section of the catalyst, endothermic steam reforming is assumed to be the predominant reaction. In this section, the wall and gas temperature drop by 70 and 40 K, respectively. Both hot spots are located slightly downstream of the oxidation zone. The shift is caused by axial heat conduction to the colder reforming zone.
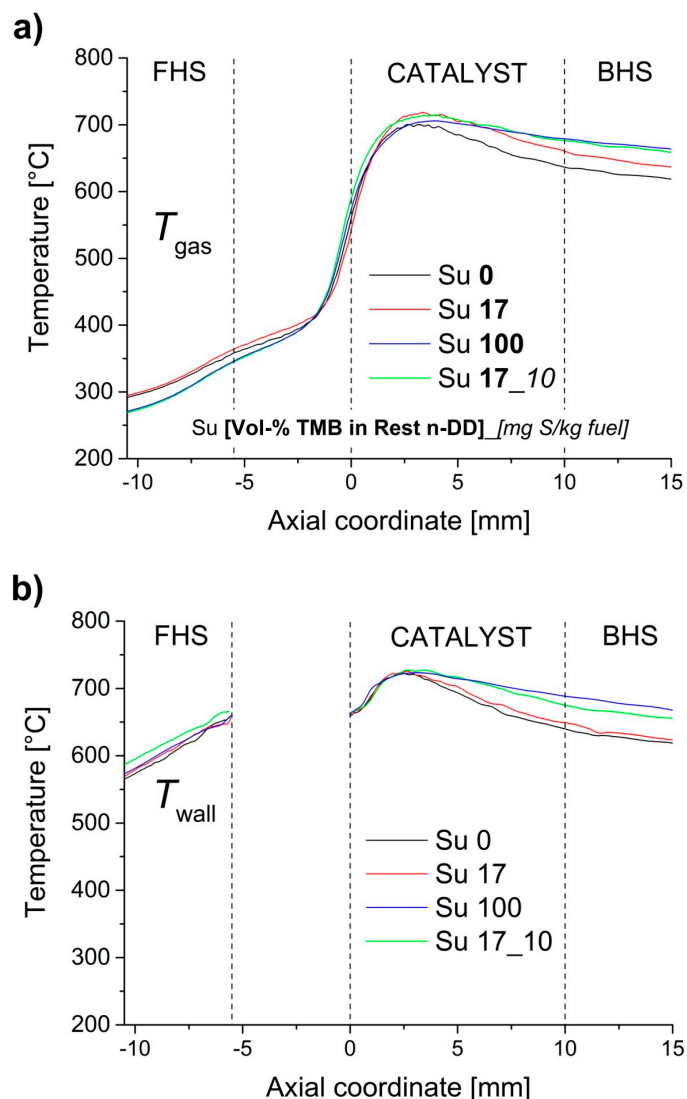
Figure 2. Gas-phase (**a**) and surface (**b**) temperature profile for the CPOX of fuel Su 17 as function of the axial coordinate *z* for the Rh catalyst (*z* = 0–10 mm). For the gas-phase temperature T_{gas}, the moving average for five points is displayed. Along the axial coordinate, the location of the front heat shield (FHS), the catalyst, and the back heat shield (BHS) is indicated.

2.2. Reaction Zones in CPOX of Higher Hydrocarbons

Compared to former studies of CPOX of methane on Rh [10,12,18,21,35] and propane on Rh [14,35], the two major observations of this study for higher hydrocarbons have not been reported: the extended region for consumption of oxygen and the delayed formation of hydrogen. For DD and all other fuels which were investigated within our study, we clearly see an indirect formation route for hydrogen via water as intermediate, as has already been suggested for e.g., high hydrocarbons [22]. In contrast to the formation of hydrogen, the other partial oxidation product, carbon monoxide, is generated right at the entrance of the catalyst, together with CO_2 and H_2O. The results obtained in this study indicate three reaction zones: the oxidation zone (0 mm < *z* < 1.5 mm), the oxy-reforming zone (1.5 mm < *z* < 3 mm) and the reforming zone (3 mm < *z* < 10 mm). In the first two reaction zones, oxygen is present. In the oxidation zone, total oxidation products are formed predominantly via total oxidation. Also, CO is generated in this zone. The molar fraction of CO shows also a local minimum at the axial position *z* = 1 mm. After the first reaction zone, no more CO_2 is produced as the molar fraction stays nearly constant in the following reaction zones. The oxy-reforming zone is located at 1.5 mm < *z* < 3 mm

with molecular oxygen still present. In this zone, H_2 is for the first time detected and CO is steadily generated. According to this observation, oxidative reaction pathways such as dehydrogenation of hydrocarbons and partial oxidation are likely. Additionally, steam reforming may occur as well, as water is consumed within this zone. The total oxidation rate here is slower than in the oxidation zone; the molar fractions of CO_2 and H_2O have already reached their maximum. The third reaction zone, the reforming zone, begins at the axial position of $z = 3$ mm and lasts until the end of the catalyst at $z = 10$ mm. In this zone, no more oxygen is detected in the gas phase. This region is dominated by steam reforming, converting hydrocarbons into syngas.

2.3. Reaction Zones in Methane CPOX

The occurrence of three reaction zones has already been postulated in a theoretical study by Maestri et al. [16] and by Beretta et al. [36] at intermediate temperatures (approx. 500 °C) and with methane as a fuel. In their reaction pathway analysis for methane partial oxidation on rhodium, three main reaction zones are identified. The first zone is dominated by total oxidation of methane to CO_2 and H_2O, and the simulations show that oxygen is the most abundant reaction intermediate (MARI) on the reaction surface [16]. They concluded that the oxidation of surface intermediates such as CO* and H* is preferred compared to their desorption. In the second reaction zone, CO* and H* are reported to be most abundant due to the much stronger mass transport limitation of oxygen, which leads to a decrease of the reaction rates of oxidation pathways [16]. The authors concluded that in the third reaction zone, in which oxygen is fully consumed, further oxidation only occurs through adsorbed OH* species originating from adsorbed water. According to their study [16], steam reforming and the water-gas shift reaction are the dominant reaction pathways in the absence of oxygen. At higher temperatures ($T > 1000$ °C), however, they report that the first zone vanishes and only the second and third zone is present. With the investigation of the CPOX of higher hydrocarbons within our study, three reaction zones can be found as well, even at higher temperatures ($T > 700$ °C).

In our system, the molar fraction profiles in the first two reaction zones differ significantly from systems in which methane is used as a fuel and Rh as catalyst. For higher hydrocarbons as a fuel, the adsorption and activation of hydrocarbons on the catalytic surface plays an important role in the first reaction zone. CO_2 and H_2O are formed as total oxidation products in this region, which is true for all studies on CPOX of hydrocarbons [10,12,14,18,21,35]. For CPOX of DD and TMB, CO generation was also observed but no hydrogen. The formation of by-products such as olefins, methane, and other dehydrogenation or cracking products in the oxidation zone (first zone) is very likely in our study on jet fuel surrogates. The by-products are not predicted or taken into account by Maestri et al. [16] as they do not occur during methane CPOX. In the second reaction zone, H_2 is observed in the gas phase for the first time, which is untypical for CPOX of methane on rhodium according to in-situ investigations by several groups [10,12,18,37,38]. In these studies, hydrogen was detected in the gas phase as early as within the first mm of the catalyst section. For the intermediate temperature of approx. 500 °C, Maestri et al. [16] also observed a delayed formation of H_2 in the second zone. However, in their study, CO formation starts also in the second zone, whereas we observe CO formation for CPOX of jet fuel surrogates already in the first zone at the catalyst inlet.

One of our previous studies, in which we compared Pd/Al_2O_3 and Rh/Al_2O_3 for methane CPOX [18], showed that the delayed formation of H_2 is also observed for methane CPOX when using Pd as catalytic material. Additionally, CO formation starts together with H_2O and CO_2 for Pd-catalyzed methane CPOX as well as for CPOX of the investigated jet fuel surrogates. For both of these combinations (CH_4/Pd, Surrogate/Rh), the area, in which oxygen is detected, is much longer (approx. 2.5–3 mm) compared to the one for methane CPOX on Rh. However, there are differences between the investigated CPOX of jet fuel surrogates on Rh and CPOX of methane on Pd, as we see a local minimum in CO molar fraction in the former case and a local minimum in CO_2 in the latter case. In studies with Pt and Pt/Rh, hydrogen and CO are shown as primary products at short contact times, whereas an influence on mass transport limitation by the variation of the catalyst geometry

has been reported [7,39]. Additionally, a direct formation towards syngas has been suggested in a TAP (temporal analysis of products) reactor, different to this study, albeit on platinum catalysts [40]. There, it was also reported that the definition of the reaction products is driven by oxygen adsorbates, showing different regimes depending on the availability of gas phase oxygen.

Similar to all of the beforehand mentioned catalysts and fuels in CPOX is the existence of the reforming zone. It has already been postulated in the literature for methane CPOX [10,12,16,18,37,38] and could be observed for higher hydrocarbons as fuels as well. The main impact of the fuel on the concentration profile is observed to be in the zone(s) in which oxygen is present in the gas phase.

2.4. Formation of by-Products for CPOX of Higher Hydrocarbons

Higher hydrocarbons have shown a tendency to form cracking products, which is mainly due to gas-phase reactions, occurring at high temperatures and fuel rich conditions [14,27,35,41]. In several studies on CPOX of higher hydrocarbons, the influence of gas-phase reactions is already unraveled on the product gas yield [22,41–43]. For instance, for CPOX of *i*-octane, a gas-phase mechanism was coupled with a detailed reaction mechanism for C1–C3 species and global reaction for adsorption of *i*-octane [22]. Here, the transfer of radicals produced at the surface to the gas bulk by radial diffusion is reported to be relevant for the occurrence of cracking products such as olefins. In Hartmann et al. [22], the simulations predicted that all major products are produced heterogeneously within the first section of the catalyst. It is confirmed in this study about jet fuel surrogates that the reaction is limited by mass-transfer of oxygen. After oxygen is completely consumed, gas-phase reactions become dominant compared to heterogeneous reactions, leading to by-product formation [22]. As these simulations were performed under isothermal conditions, a potential temperature hot spot at the entrance of the catalyst was not considered, which may have influenced the calculations.

The conditions of this study were chosen to avoid gas-phase reactions by using low reactant concentration and lean conditions (excess of oxygen regarding CPOX stoichiometry (C/O = 0.75)). Nevertheless, at high temperatures, we believe that the gas-phase reactions contribute to the by-product formation significantly in the first two reaction zones as proposed for propane by several groups for Rh [14,36,44]. There, cracking or dehydrogenation reaction products such as ethylene and propylene as well as methane and acetylene are formed near the entrance of the catalyst, where the temperature reaches its maximum [44]. Concerning spatially resolved concentration profiles, the formation of these cracking products was experimentally confirmed in the first few mm of the catalyst [14]. There, the profiles of the olefins ethylene and propylene show a maximum at approx. 2 mm, and are fully converted downstream of the catalyst via steam reforming. In our study, however, by-product formation (e.g., methane, ethylene, lower hydrocarbons) could not be experimentally verified due to the high detection limit of the system (50–100 ppm depending on the species). However, the calculation of molar balances concerning oxygen, carbon, and hydrogen indicate the formation of by-products in the hottest zone of the catalyst, but with concentrations below the lower detection limit of the system. The oxygen balance shows a deviation of 10% for all fuels along the length of the catalyst. At the catalyst outlet, the molar balance for C and H is close to within 15%. However, along the axial coordinate, the molar balance shows a local decline (-0.5 mm $< z <$ 5 mm) in the order of 30% for the C-balance and of 26% for the H-balance (not shown). As these products could not be detected by the analytical method, they were not taken into account for the balance calculation. Nevertheless, we expect for Su 17 as well as for the other fuels that this region is affected by cracking and dehydrogenation re actions, leading to unsaturated and lower saturated hydrocarbons. In the first few mm of the first reaction zone, CO is slightly consumed. In this region, oxidation and desorption of unsaturated hydrocarbons will be favored and lead to a slower oxidation rate, suggesting that either olefins or intermediates (e.g., CO as a partial oxidation product) are adsorbed strongly on the catalyst surface, causing self-inhibition and hence, the slight local decline in CO. Such difference in behavior of hydrocarbons was observed in oxidation studies of propylene and propane over noble metal catalysts [45].

In addition to that, as a local decline in the molar carbon and hydrogen balance at the position of the maxima in x_{H_2O}, x_{CO_2}, and the minimum in x_{CO} could be calculated, very complex reactions play a role in the conversion process of high hydrocarbons including by-product formation. Apart from oxidation reactions, the composition of these products and hydrogen is driven by the Boudouard reaction (1), water-gas shift reaction (2), and methanation (3) [46–48].

$$CO_{2(g)} + C_{(s)} \rightleftharpoons 2CO_{(g)} \tag{1}$$

$$CO + H_2O \rightleftharpoons CO_2 + H_2 \tag{2}$$

$$CO + 3H_2 \rightleftharpoons CH_4 + H_2O \tag{3}$$

As a slight local net CO consumption was observed, the Boudouard reaction as a CO sink is likely, despite being in a temperature regime, in which local CO-production should be favored [46]. However, as in the relevant region, oxidation reactions through adsorbed oxygen will very likely prevent the continuous presence of solid carbon, which is relevant for the first reaction zone [16]. Therefore, the Boudouard reaction is driven by the local carbon consumption towards additional local CO-consumption. The water-gas shift reaction could also affect the CO profile and could cause the observed CO sink as hydrogen is not detected as the main product in this region. It has to be taken into account that radial concentration profiles are not detectable with our method. Therefore, although oxygen is still detected in the gas phase, a methanation route for the local CO consumption must be taken into consideration, as a local oxygen depletion is strongly mass-transport limited and oxygen is likely completely consumed in the boundary layer close to the catalyst. Nevertheless, further experiments and confirmation by CFD-(computational fluid dynamics) modeling is needed to explain this unexpected behavior as experimental evidence of by-product formation in this region is crucial for additional evaluation of the reaction pathways, relevant for this local CO-consumption. Due to the high gas-phase temperature of 716 °C and the deviation of the balances, the formation of lower hydrocarbons, including methane, ethylene, acetylene, or other saturated and unsaturated hydrocarbons as well as solid carbon formation, is expected in the first two reaction zones. In the reaction zone further downstream, in which oxygen is completely consumed, all types of hydrocarbons are converted by the dominant steam reforming reaction [12,18,21,37,49].

2.5. Influence of Aromatic and Sulfur Content

In Figures 3 and 4, the axial concentration profiles for the different blends are displayed. In the following section, we highlight the variation in behavior for the different surrogates.

The variation of the carbon chain length leads to variation of the inlet concentration of oxygen and hydrocarbons to keep the total reactant concentration constant. The C/O-ratio of 0.75 could be reproduced for all inlet and outlet conditions within 12%, which support the precision of the detection of main reaction components. In Figure 3, the reactant concentration is displayed. There, the oxygen inlet concentration rises and the hydrocarbon inlet concentration declines with longer carbon chain length, which is trivial due to the chosen inlet conditions of C/O = 0.75 and the fixed total reactant concentration of 5%. Additionally, as the two fuels with very similar composition, Su 17 and Su 17_10, show a nearly identical profile for oxygen as well as fuel in Figure 3, the reliability of the set-up and the sampling procedure is verified.

Comparing the molar fractions of CO_2 for all different fuels (Figure 4b), no influence of the fuel on the local production of CO_2 could be observed despite the various C/H ratios, the different species, and the sulfur content of the fuels. The only exception is Su 100, for which the CO_2, H_2O, and CO generation already starts upstream of the catalyst at a position of approx. −0.5 mm. This difference in behavior for Su 100 is believed to be caused by a combination of gas-phase decomposition of 1,2,4-trimethylbenzene and upstream axial diffusion of the products, the latter is confirmed by CFD-studies for CPOX of methane [38]. A slight decrease from x_{CO_2} = 0.0195 (z = 1.75 mm) to

x_{CO_2} = 0.018 (z = 10 mm) was observed for pure dodecane (Su 0, Figure 4b). The cause could be dry reforming on the last two millimeters of the catalyst or a mixing effect when the gases enter the back heat shield (BHS) and the gases of different channels mix in the probed channel of the BHS. The water-gas shift reaction is unlikely as H_2 increases at the same position as CO_2 decreases.

An influence of the aromatic content can be observed by comparing the molar fractions of CO (Figure 4a). Especially within the first 2 mm of the catalyst, a trend of increasing mole fractions of CO at a fixed position could be observed for rising aromatic content of the fuel. In all cases, CO is partly consumed between the axial positions 0.25 and 1.25 mm. As explained in the previous section, we assume that an interplay of the Boudouard reaction, the formation of by-products, and methanation is responsible for the CO consumption at this position. After the local minimum of CO, a steady increase of the molar fraction of CO results in a similar trend in the molar fractions of all fuels with aromatic content. For dodecane, however, a higher molar fraction of CO of x_{CO} = 0.035 (z = 10 mm) compared to x_{CO} = 0.027 (z = 10 mm) for fuels containing TMB was observed. With increasing amount of paraffin in the fuel, the molar fraction of hydrogen (Figure 4c) increases from x_{H_2} (Su 100) = 0.023 to x_{H_2} (Su 0) = 0.042 (both at z = 10 mm). This behavior was expected due to the higher hydrogen content of the paraffin. This trend was also observed for water formation in the first two reaction zones, where the molar fraction of water (Figure 4d) reaches its maximum value for all fuels. The maximum in molar fraction of water rises with an increasing hydrogen content of the fuel. For fuels with high aromatic content, we expect a rising coking tendency, which could contribute to the decreasing hydrogen molar fraction with increasing aromatic content. In general, this is confirmed for other alkanes or aromatic compounds in CPOX, which was reported by other groups [27,41].

In the third reaction zone, the reforming zone, in which steam reforming is the predominant reaction pathway and in which oxygen is already depleted, the influence of tiny amounts of sulfur in the fuel becomes relevant for the reaction sequence of the CPOX for all investigated surrogates. Lower local water consumption was observed for the sulfur-containing fuel, Su 17_10 compared to its sulfur-free counterpart Su 17. For Su 17_10, 45% of the maximum value of the molar fraction of water is consumed between the axial positions of z = 2.0 mm and 10 mm. For the sulfur-free equivalent Su 17, a decline of the molar fraction of water by 50% was observed. This leads to a lower hydrogen local production of x_{H_2} (Su 17_10) = 3.0% compared to x_{H_2} (Su 17) = 3.3%. In this catalytic region, sulfur tends to have the largest impact on the reaction system, leading to less steam reforming. The concentration profiles show similar trends for all fuels in the region, in which oxygen is present in the gas phase. Owing to the highly oxophilic rhodium (compared to other noble metals), chemisorption of oxygen as well as aromatics prevented sulfur poisoning, as proposed in [26]. A modification of the support has been already identified as an option in the literature for increasing the oxygen ion conductivity, not only in order to prevent catalyst poisoning by sulfur, but also to support the resistance of the catalyst to coke formation [28].

The temperature profiles of all fuels show a hot spot in the gas phase and at the wall at around 2.5 mm (Figure 2). The hot spot of the wall temperature has the same value for all fuels: $T_{wall,max}$ = 725 °C. In the region of the hot spot, homogeneous cracking reactions of the hydrocarbons due to high temperatures could occur in addition to heterogeneous dehydrogenation or cracking reactions. As the calculated molar balances indicate at z = −0.5–5 mm an amount of hydrogen and carbon, which is not accounted for by the detected species, a variety of hydrocarbons, including methane and ethylene, are likely to be present in this zone. Measurements with higher reactant concentration support this observation, as significant amounts of methane (~800 ppm) and other by-products (~150 ppm) were generated at the catalyst outlet, especially for fuels with higher sulfur content compared to Su 17_10 and for a higher amount reactive gases of 10% [34]. The temperature profiles show a decrease in temperature downstream of the hot spot, at z > 2.5 mm. The total decline in temperature up to the position of z = 10 mm is lower for the sulfur-containing surrogate Su 17_10 (T_{wall} = 674 °C, z = 10 mm) and for the pure aromatic fuel Su 100 (T_{wall} = 688 °C, z = 10 mm) than that of both Su 0 (T_{wall} = 640 °C, z = 10 mm) and Su 17 (T_{wall} = 649 °C, z = 10 mm). This observation

indicates that, in the oxy-reforming and reforming zone, the rates for endothermic reactions, such as steam reforming, are slower for Su 17_10 and Su 100 as a consequence of higher by-product formation and, hence, coke deposition. Additionally, *n*-dodecane and 1,2,4-trimethylbenzene have different tendencies for gas-phase reactions due to their different molecular structure. In general, radical formation can be stabilized by the aromatic ring of a molecule such as 1,2,4-trimethylbenzene, which enhances the stability of the molecule compared to alkanes [50]. For fuel conservation in the military aircraft sector, additives with high thermal stability show a similar radical stabilization [51–53]. Due to this enhanced stability of the C–C-bonding, dodecane is more reactive towards CPOX compared to 1,2,4-trimethylbenzene and is therefore consumed at a higher rate. This is supported by various experiments with different hydrocarbon structure [27,41]. Additionally, slower decomposition of the formed hydrocarbons and the fuel in the absence of oxygen due to coke formation in the reforming zone is likely. As a consequence, a lower rate in steam reforming would result in a lower local consumption of water, which is confirmed when comparing the concentration profiles of H_2O for these fuels (Figure 4d). With a slower rate in steam reforming, there will be a higher by-product concentration at the catalyst outlet as a lower amount of the remaining hydrocarbons including reactants and by-products are consumed.
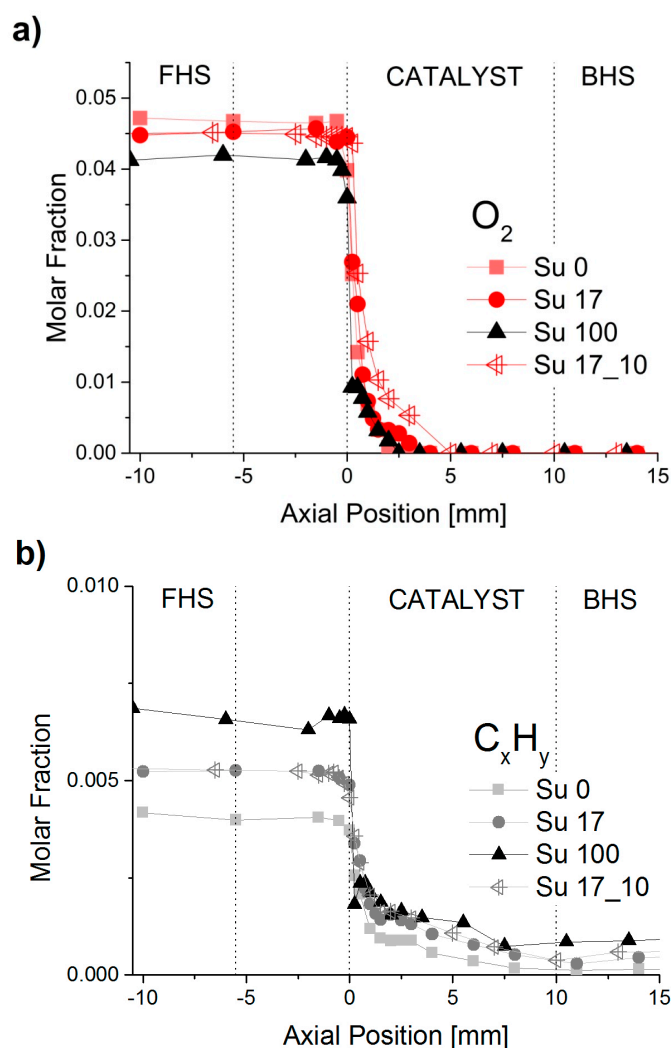

Figure 3. Molar fraction of the reactants oxygen (**a**) and fuel (**b**) as function of the axial coordinate *z* for the Rh catalyst (*z* = 0–10 mm) for the CPOX of different surrogates. The molar fraction of oxygen for Su 17_10 was calculated based on oxygen balance. Along the axial coordinate, the location of the front heat shield (FHS), the catalyst, and the back heat shield (BHS) is indicated.
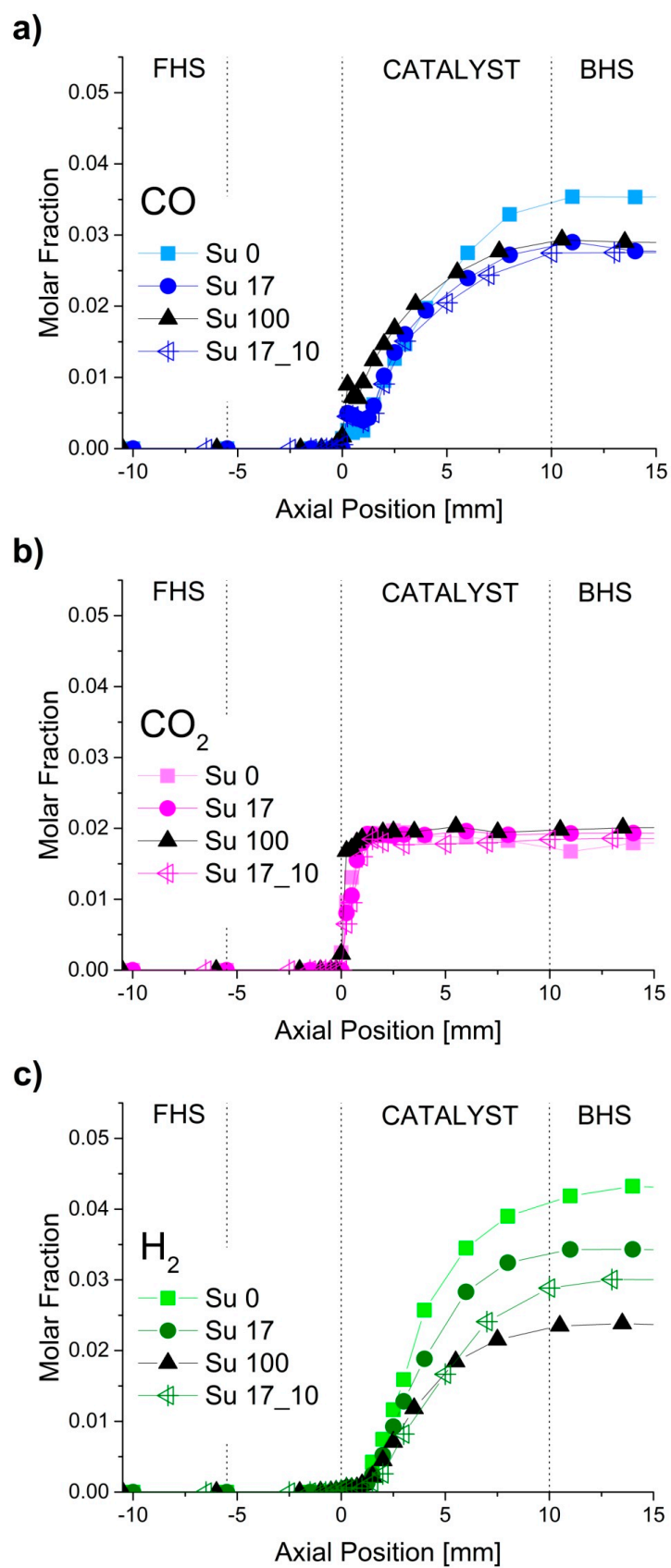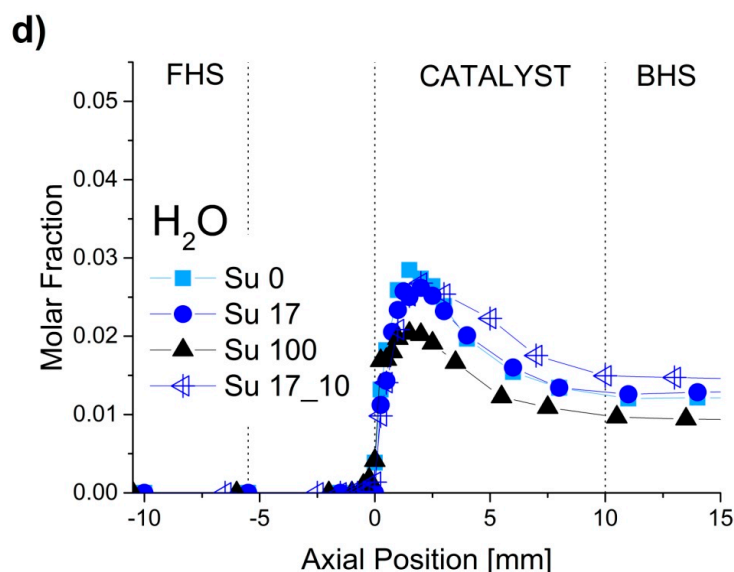
a)

b)

c)

Figure 4. *Cont.*

Figure 4. Molar fraction of the products carbon monoxide (**a**); carbon dioxide (**b**); hydrogen (**c**) and water (**d**) as function of the axial coordinate *z* for the Rh catalyst (*z* = 0–10 mm) for CPOX of different surrogates. Along the axial coordinate, the location of the front heat shield (FHS), the catalyst, and the back heat shield (BHS) is indicated.

3. Materials and Methods

All experiments were conducted in a quartz tube reactor, which is placed in a furnace for thermal insulation and preheating for light-off. A molar C/O-ratio of 0.75, a total volume flow of 4 slpm (standard liters per minute) and 95% dilution in N_2 were used. For the calculation of the C/O-ratio at the given inlet conditions, the molar amount of carbon atoms entering the reactor are related to the molar amount of oxygen atoms entering the reactor. These conditions result in a total reactive flow of 5%, i.e., 0.2 slpm, a residence time of the order of 10 ms, and a gas-hourly space velocity (GHSV) of 120,000 h^{-1} at standard conditions (*T* = 298 K, *p* = 1 atm). The catalytic honeycomb monolith with a Rh/Al_2O_3 washcoat was 19 mm in diameter, 10 mm in length with 600 cpsi (channels per square inch). The experiments are taken within 10 hours' time on stream. Within this time, the distribution of the reaction products was stable for all fuels, as experimentally confirmed in our previous study [34]. All used fuels were evaporated upstream of the reactor by means of a combination of a CORI-flow (Bronkhorst High-Tech, Ruurlo, The Netherlands) and a CEM (Controlled Evaporator Mixer, Bronkhorst High-Tech). The gases were preheated to 190 °C and the furnace was kept at 300 °C maintaining a steady temperature around the quartz tube reactor, which led to quasi-autothermal operation. For light-off, a diluted mixture of H_2 and O_2 was fed to the reactor before the fuel was switched to the hydrocarbon/oxygen mixture. Four different fuels were used: the pure substances, *n*-dodecane (DD; Su 0) and 1,2,4-trimethylbenzene (TMB, Su 100), a blend of 17 vol % TMB and 83 vol % DD with (Su 17_10) and without (Su 17) addition of benzothiophene. The amount of benzothiophene for the fuel Su 17_10 was calculated to be 10 mg S in 1 kg fuel. The commercial honeycomb catalyst was placed between two heat shields, consisting of uncoated monolith (cordierite) in the quartz tube reactor. Upstream of the catalyst, a void space of 5 mm was kept between the front heat shield and the catalyst to achieve better flow uniformity (Figure 5).
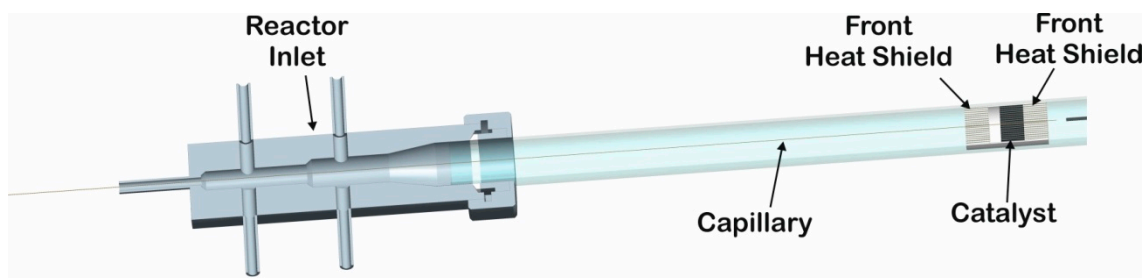
Figure 5. Scheme of the reactor setup with reactor inlet, capillary, front heat shield (FHS), catalyst (CAT), and back heat shield (BHS). The *z*-axis goes axially through the cylindrical quartz reactor, with *z* = 0 mm as the catalyst inlet and 10 mm as the catalyst outlet.

The in-situ sampling technique is similar to those introduced by Partridge et al. [54], Horn [10] and Donzazzi et al. [14,37]. The sampling technique is used to collect spatially-resolved concentration and temperature profiles within a catalytic channel of a honeycomb monolith, which is in a laminar flow regime. A capillary (inner diameter = 100 μm, outer diameter = 170 μm) was moved stepwise through the central channel along the axial coordinate inside a channel of the catalyst (Figure 5). At each axial position inside and outside the catalyst, a gas sample was continuously sucked into the capillary at a sucking rate of ~0.5–1 Ncc/min and collected in a sampling loop. The sample was periodically purged from the loop into the analytic section, analyzing the gas composition at the current position of the capillary. The analytics consisted of a FTIR analyzer (MKS Multigas 2030, MKS instruments, Andover, Massachusetts, USA), IMR-MS (Airsense, V&F Analysentechnik GmbH, Absam, Austria), and EI-MS (H-Sense, V&F), detecting all relevant main products of the CPOX of hydrocarbons, including all C1-species, H_2, H_2O, and O_2. For the higher hydrocarbons, a method was used in order to detect H-C vibrations of all higher hydrocarbons in the FTIR. This method is not capable of distinguishing between different higher hydrocarbons such as *n*-dodecane and 1,2,4-trimethylbenzene or their cracking products. Nevertheless, in order to display the profile of the fuel as reactant, the method was applicable, as the deviation stayed within the total error of the system. Additionally, due to the low concentration of the reactive flow and the lower detection limit of the sampling system (50–100 ppm depending on the species), by-products such as ethylene and methane could not be detected for the studied cases. At each axial position, three analyses were carried out. The element balances typically closed within ±5%–10%. The limitations of the sampling technique, in particular the effect of the capillary on the flow field and residence time inside a channel has already been addressed elsewhere [38]. These limitations, however, do not affect any qualitative conclusions drawn in this study. For a detailed description of our reactor set-up and sampling technique, we refer to our previous articles [21,38].

The gas-phase T_{gas} and surface temperature T_{wall} profiles are collected inside a central channel of the catalyst by means of a thermocouple and an optical fiber connected to a pyrometer, respectively. The temperature probes are inserted into a capillary (outer diameter: 630 μm) as a guideway and to prevent contact of the reactive gases with the temperature probes. The capillary was moved along the channel by a miniature motorized linear stage (Zaber Technologies, T-LSM100A, Vancouver, British Columbia, Canada) with a high spatial resolution. A spatial resolution of 0.25 mm was obtained for the collection of the concentration profile. A higher resolution of 0.089 mm was reached for the temperature profiles. Thermodynamic equilibrium calculations were performed with the software package DETCHEM^{EQUIL} (Version 2.5, Karlsruhe, Germany, 2014) [55] under isothermal conditions, using dodecane and trimethylbenzene as model species for the calculations.

4. Conclusions

In this study, insights into the reaction system of the catalytic partial oxidation of various mixtures of *n*-dodecane and 1,2,4-trimethylbenzene with and without addition of benzothiophene are provided. The spatially-resolved concentration and temperature profiles reveal a general behavior of jet fuel surrogates, the differences between the different surrogates, and allow for a comparison with in-situ studies on the CPOX of methane.

In the case of jet fuel surrogates, we observe three different reaction zones inside the catalyst. The oxidation zone ($z = 0$–1.5 mm) is dominated by total oxidation of the hydrocarbons to carbon dioxide, steam, and carbon monoxide production. In the oxy-reforming zone ($z = 1.5$–3 mm), in which oxygen is still available, a local consumption of CO was observed and the formation of H_2 started. The local CO consumption is very likely due to a combination of methanation, a slower dehydrogenation process, and the Boudouard reaction. The formation of hydrogen starting in the second reaction zone indicates the indirect mechanism for the formation of hydrogen for jet fuel surrogates. The reforming zone ($z = 3$–10 mm) is characterized by the absence of molecular oxygen, which has already been completely consumed. Endothermic steam reforming is the predominant reaction in this zone.

The delayed formation of hydrogen differs from studies performed for methane CPOX on Rh [10,12,18,37,38], in which hydrogen is already detected within the first section of the catalyst. A shifted hydrogen formation was, however, observed for methane CPOX on Pd [18]. Additionally, the consumption of oxygen stretches over a longer area of the catalyst for jet fuel surrogates and for methane CPOX on Pd than for methane CPOX on Rh. Thus, the observed concentration profiles for the CPOX of jet fuel surrogates on Rh are more similar to ones for methane CPOX on Pd than to ones for methane CPOX on Rh. The local minimum in CO molar fraction is a unique characteristic of the CPOX of jet fuels surrogates on Rh and not observed in any of the other studies.

The investigated surrogates show the expected decrease in hydrogen formation for increasing aromatic content caused by the lower C/H ratio in the surrogates and probably by coke deposition. Homogeneous decomposition of the hydrocarbon upstream of the catalyst is only observed for the pure aromatic compound.

Comparison of the spatially-resolved profiles for a sulfur-free and the corresponding sulfur-containing surrogate disclose the influence on sulfur. Even tiny amounts of sulfur (10 ppm S per 1 kg fuel) affect the third reaction zone ($z = 3$–10 mm) by blocking active catalytic sites relevant for steam reforming. This sulfur poisoning leads to a higher molar fraction of water and a lower one of hydrogen at the catalyst outlet. The presence of oxygen in the first two zones seems to prevent blocking of active sites by sulfur. The carbon main product distribution (CO/CO_2) remains unaffected by sulfur addition. The addition of sulfur in the reactant gas flow will likely lead to more by-product formation, which was already observed in our previous ex-situ investigations for jet fuel surrogates [34]. The low concentration of by-products and the lower detection limit of the sampling system prevented a quantification of the by-product formation along the channel. For the application of sulfur-containing jet fuels in CPOX reformers, catalysts with higher resistance against sulfur poisoning, e.g., by changing the support to increase oxygen ion conductivity, are crucial to reach high hydrogen molar fractions.

Author Contributions: Claudia Antinori and Olaf Deutschmann are responsible for the experimental set-up. Julian N. Bär conducted the project, developed the measurement strategy, and performed the experiments. Julian N. Bär, Claudia Antinori, and Lubow Maier analyzed the data. All authors contributed to the discussion of the results and wrote the paper. Olaf Deutschmann was the principal investigator of the project.

Conflicts of Interest: The authors declare no conflict of interest.

References

1. Aicher, T.; Lenz, B.; Gschnell, F.; Groos, U.; Federici, F.; Caprile, L.; Parodi, L. Fuel processors for fuel cell APU applications. *J. Power Sources* **2006**, *154*, 503–508. [CrossRef]
2. Cheekatamarla, P.K.; Finnerty, C.M. Synthesis gas production via catalytic partial oxidation reforming of liquid fuels. *Int. J. Hydrogen Energy* **2008**, *33*, 5012–5019. [CrossRef]
3. Lindström, B.; Karlsson, J.A.J.; Ekdunge, P.; De Verdier, L.; Häggendal, B.; Dawody, J.; Nilsson, M.; Pettersson, L.J. Diesel fuel reformer for automotive fuel cell applications. *Int. J. Hydrogen Energy* **2009**, *34*, 3367–3381. [CrossRef]
4. Kaltschmitt, T.; Deutschmann, O. Fuel processing for fuel cells. *Adv. Chem. Eng.* **2012**, *41*, 1–64.
5. Pasel, J.; Samsun, R.C.; Peters, R.; Stolten, D. Fuel processing of diesel and kerosene for auxiliary power unit applications. *Energy Fuels* **2013**, *27*, 4386–4394. [CrossRef]
6. Xu, X.; Li, P.; Shen, Y. Small-scale reforming of diesel and jet fuels to make hydrogen and syngas for fuel cells: A review. *Appl. Energy* **2013**, *108*, 202–217. [CrossRef]
7. Hickman, D.A.; Schmidt, L.D. Production of syngas by direct catalytic oxidation of methane. *Science* **1993**, *259*, 343–346. [CrossRef] [PubMed]
8. Schwiedernoch, R.; Tischer, S.; Correa, C.; Deutschmann, O. Experimental and numerical study on the transient behavior of partial oxidation of methane in a catalytic monolith. *Chem. Eng. Sci.* **2003**, *58*, 633–642. [CrossRef]
9. Eriksson, S.; Nilsson, M.; Boutonnet, M.; Järås, S. Partial oxidation of methane over rhodium catalysts for power generation applications. *Catal. Today* **2005**, *100*, 447–451. [CrossRef]
10. Horn, R.; Williams, K.A.; Degenstein, N.J.; Schmidt, L.D. Syngas by catalytic partial oxidation of methane on rhodium: Mechanistic conclusions from spatially resolved measurements and numerical simulations. *J. Catal.* **2006**, *242*, 92–102. [CrossRef]
11. Bitsch-Larsen, A.; Degenstein, N.J.; Schmidt, L.D. Effect of sulfur in catalytic partial oxidation of methane over Rh–Ce coated foam monoliths. *Appl. Catal. B* **2008**, *78*, 364–370. [CrossRef]
12. Bitsch-Larsen, A.; Horn, R.; Schmidt, L.D. Catalytic partial oxidation of methane on rhodium and platinum: Spatial profiles at elevated pressure. *Appl. Catal. A* **2008**, *348*, 165–172. [CrossRef]
13. Christian Enger, B.; Lødeng, R.; Holmen, A. A review of catalytic partial oxidation of methane to synthesis gas with emphasis on reaction mechanisms over transition metal catalysts. *Appl. Catal. A* **2008**, *346*, 1–27. [CrossRef]
14. Donazzi, A.; Livio, D.; Maestri, M.; Beretta, A.; Groppi, G.; Tronconi, E.; Forzatti, P. Synergy of homogeneous and heterogeneous chemistry probed by in situ spatially resolved measurements of temperature and composition. *Angew. Chem. Int. Ed.* **2011**, *50*, 3943–3946. [CrossRef] [PubMed]
15. Chakrabarti, R.; Kruger, J.S.; Hermann, R.J.; Blass, S.D.; Schmidt, L.D. Spatial profiles in partial oxidation of methane and dimethyl ether in an autothermal reactor over rhodium catalysts. *Appl. Catal. A* **2014**, *483*, 97–102. [CrossRef]
16. Maestri, M.; Vlachos, D.; Beretta, A.; Forzatti, P.; Groppi, G.; Tronconi, E. Dominant reaction pathways in the catalytic partial oxidation of CH_4 on Rh. *Top. Catal.* **2009**, *52*, 1983–1988. [CrossRef]
17. Nogare, D.D.; Degenstein, N.J.; Horn, R.; Canu, P.; Schmidt, L.D. Modeling spatially resolved data of methane catalytic partial oxidation on Rh foam catalyst at different inlet compositions and flowrates. *J. Catal.* **2011**, *277*, 134–148. [CrossRef]
18. Diehm, C.; Deutschmann, O. Hydrogen production by catalytic partial oxidation of methane over staged Pd/Rh coated monoliths: Spatially resolved concentration and temperature profiles. *Int. J. Hydrogen Energy* **2014**, *39*, 17998–18004. [CrossRef]
19. Wang, D.; Dewaele, O.; Groote, A.M.D.; Froment, G.F. Reaction mechanism and role of the support in the partial oxidation of methane on Rh/Al_2O_3. *J. Catal.* **1996**, *159*, 418–426. [CrossRef]
20. Mallens, E.P.J.; Hoebink, J.H.B.J.; Marin, G.B. The reaction mechanism of the partial oxidation of methane to synthesis gas: A transient kinetic study over rhodium and a comparison with platinum. *J. Catal.* **1997**, *167*, 43–56. [CrossRef]
21. Livio, D.; Diehm, C.; Donazzi, A.; Beretta, A.; Deutschmann, O. Catalytic partial oxidation of ethanol over Rh/Al_2O_3: Spatially resolved temperature and concentration profiles. *Appl. Catal. A* **2013**, *467*, 530–541. [CrossRef]

22. Hartmann, M.; Maier, L.; Minh, H.D.; Deutschmann, O. Catalytic partial oxidation of iso-octane over rhodium catalysts: An experimental, modeling, and simulation study. *Combust. Flame* **2010**, *157*, 1771–1782. [CrossRef]

23. Curran, H.J.; Gaffuri, P.; Pitz, W.J.; Westbrook, C.K. A comprehensive modeling study of iso-octane oxidation. *Combust. Flame* **2002**, *129*, 253–280. [CrossRef]

24. Krummenacher, J.J.; West, K.N.; Schmidt, L.D. Catalytic partial oxidation of higher hydrocarbons at millisecond contact times: decane, hexadecane, and diesel fuel. *J. Catal.* **2003**, *215*, 332–343. [CrossRef]

25. Cheekatamarla, P.K.; Lane, A.M. Catalytic autothermal reforming of diesel fuel for hydrogen generation in fuel cells: I. Activity tests and sulfur poisoning. *J. Power Sources* **2005**, *152*, 256–263. [CrossRef]

26. Shekhawat, D.; Gardner, T.H.; Berry, D.A.; Salazar, M.; Haynes, D.J.; Spivey, J.J. Catalytic partial oxidation of n-tetradecane in the presence of sulfur or polynuclear aromatics: Effects of support and metal. *Appl. Catal. A* **2006**, *311*, 8–16. [CrossRef]

27. Hartmann, M.; Kaltschmitt, T.; Deutschmann, O. Catalytic partial oxidation of higher hydrocarbon fuel components on Rh/Al_2O_3 coated honeycomb monoliths. *Catal. Today* **2009**, *147*, S204–S209. [CrossRef]

28. Haynes, D.J.; Berry, D.A.; Shekhawat, D.; Spivey, J.J. Catalytic partial oxidation of *n*-tetradecane using Rh and Sr substituted pyrochlores: Effects of sulfur. *Catal. Today* **2009**, *145*, 121–126. [CrossRef]

29. Shekhawat, D.; Berry, D.A.; Haynes, D.J.; Spivey, J.J. Fuel constituent effects on fuel reforming properties for fuel cell applications. *Fuel* **2009**, *88*, 817–825. [CrossRef]

30. DuBois, T.G.; Nieh, S. Selection and performance comparison of jet fuel surrogates for autothermal reforming. *Fuel* **2011**, *90*, 1439–1448. [CrossRef]

31. Diehm, C.; Kaltschmitt, T.; Deutschmann, O. Hydrogen production by partial oxidation of ethanol/gasoline blends over Rh/Al_2O_3. *Catal. Today* **2012**, *197*, 90–100. [CrossRef]

32. Granlund, M.Z.; Jansson, K.; Nilsson, M.; Dawody, J.; Pettersson, L.J. Evaluation of Co, La, and Mn promoted Rh catalysts for autothermal reforming of commercial diesel. *Appl. Catal. B* **2014**, *154–155*, 386–394. [CrossRef]

33. Granlund, M.Z.; Jansson, K.; Nilsson, M.; Dawody, J.; Pettersson, L.J. Evaluation of Co, La, and Mn promoted Rh catalysts for autothermal reforming of commercial diesel: Aging and characterization. *Appl. Catal. B* **2015**, *172–173*, 145–153. [CrossRef]

34. Bär, J.N.; Rocha, M.I.; Oliviera, E.J.; Deutschmann, O. Impact of sulfur on catalytic partial oxidation of jet fuel surrogates over Rh/Al_2O_3. *Int. J. Hydrogen Energy* **2015**, *41*, 3701–3711. [CrossRef]

35. Livio, D.; Donazzi, A.; Beretta, A.; Groppi, G.; Forzatti, P. Experimental and modeling analysis of the thermal behavior of an autothermal C_3H_8 catalytic partial oxidation reformer. *Ind. Eng. Chem. Res.* **2012**, *51*, 7573–7583. [CrossRef]

36. Beretta, A.; Donazzi, A.; Groppi, G.; Maestri, M.; Tronconi, E.; Forzatti, P. Gaining insight into the kinetics of partial oxidation of light hydrocarbons on Rh, through a multiscale methodology based on advanced experimental and modeling techniques. *Catalysis* **2013**, *25*, 1–49.

37. Donazzi, A.; Livio, D.; Beretta, A.; Groppi, G.; Forzatti, P. Surface temperature profiles in CH_4 CPO over honeycomb supported Rh catalyst probed with in situ optical pyrometer. *Appl. Catal. A* **2011**, *402*, 41–49. [CrossRef]

38. Hettel, M.; Diehm, C.; Torkashvand, B.; Deutschmann, O. Critical evaluation of in situ probe techniques for catalytic honeycomb monoliths. *Catal. Today* **2013**, *216*, 2–10. [CrossRef]

39. Hickman, D.A.; Schmidt, L.D. Synthesis gas formation by direct oxidation of methane over Pt monoliths. *J. Catal.* **1992**, *138*, 267–282. [CrossRef]

40. Fathi, M.; Monnet, F.; Schuurman, Y.; Holmen, A.; Mirodatos, C. Reactive oxygen species on platinum gauzes during partial oxidation of methane into synthesis gas. *J. Catal.* **2000**, *190*, 439–445. [CrossRef]

41. Subramanian, R.; Panuccio, G.J.; Krummenacher, J.J.; Lee, I.C.; Schmidt, L.D. Catalytic partial oxidation of higher hydrocarbons: reactivities and selectivities of mixtures. *Chem. Eng. Sci.* **2004**, *59*, 5501–5507. [CrossRef]

42. Hartmann, M.; Maier, L.; Deutschmann, O. Hydrogen production by catalytic partial oxidation of iso-octane at varying flow rate and fuel/oxygen ratio: From detailed kinetics to reactor behavior. *Appl. Catal. A* **2011**, *391*, 144–152. [CrossRef]

43. Kaltschmitt, T.; Maier, L.; Hartmann, M.; Hauck, C.; Deutschmann, O. Influence of gas-phase reactions on catalytic reforming of isooctane. *Proc. Combust. Inst.* **2011**, *33*, 3177–3183. [CrossRef]

44. Aartun, I.; Silberova, B.; Venvik, H.; Pfeifer, P.; Görke, O.; Schubert, K.; Holmen, A. Hydrogen production from propane in Rh-impregnated metallic microchannel reactors and alumina foams. *Catal. Today* **2005**, *105*, 469–478. [CrossRef]

45. Shinjoh, H.; Muraki, H.; Fujitani, Y. Periodic operation effects in propane and propylene oxidation over noble metal catalysts. *Appl. Catal.* **1989**, *49*, 195–204. [CrossRef]

46. Calo, J.M.; Perkins, M.T. A heterogeneous surface model for the "steady-state" kinetics of the Boudouard reaction. *Carbon* **1987**, *25*, 395–407. [CrossRef]

47. Lim, J.Y.; McGregor, J.; Sederman, A.J.; Dennis, J.S. The role of the Boudouard and water–gas shift reactions in the methanation of CO or CO_2 over Ni/γ-Al_2O_3 catalyst. *Chem. Eng. Sci.* **2016**, *152*, 754–766. [CrossRef]

48. Antonio, G.F.M.; Franco, F.; Batalha, N.; Pereira, M.M. Coupling CH_4 pyrolysis with CO_2 activation via reverse Boudouard reaction in the presence of O_2 trhough a multifunctional catalyst Ni-V-Li/Al_2O_3. *J. CO_2 Util.* **2016**, *16*, 458–465. [CrossRef]

49. Deutschmann, O.; Grunwaldt, J.-D. Exhaust gas aftertreatment in mobile systems: Status, challenges, and perspectives. *Chem. Ing. Tech.* **2013**, *85*, 595–617. [CrossRef]

50. Pryor, W. *Frontiers of Free Radical Chemistry*; Elsevier Science: Amsterdam, The Netherlands, 2012.

51. Hazlett, R.N. *Thermal Oxidation Stability of Aviation Turbine Fuels*; ASTM: West Conshohocken, PA, USA, 1991.

52. Yoon, E.M.; Selvaraj, L.; Song, C.; Stallman, J.B.; Coleman, M.M. High-temperature stabilizers for jet fuels and similar hydrocarbon mixtures. 1. Comparative studies of hydrogen donors. *Energy Fuels* **1996**, *10*, 806–811. [CrossRef]

53. Yoon, E.M.; Selvaraj, L.; Eser, S.; Coleman, M.M. High-temperature stabilizers for jet fuels and similar hydrocarbon mixtures. 2. Kinetic studies. *Energy Fuels* **1996**, *10*, 812–815. [CrossRef]

54. Partridge, W.P.; Storey, J.M.; Lewis, S.; Smithwick, R.; DeVault, G.L.; Cunningham, M.J.; Currier, N.; Yonushonis, T.M. Time-resolved measurements of emission transients by mass spectrometry. *SAE Tech. Paper* **2000**, 2000-01-2952. [CrossRef]

55. Deutschmann, O.; Tischer, S.; Correa, C.; Chatterjee, D.; Kleditzsch, S.; Janardhanan, V.M.; Mladenov, N.; Minh, H.D.; Karadeniz, H.; Hettel, M. *DETCHEM^{TM} Software Package*, Version 2.5; DETCHEM: Karlsruhe, Germany, 2014.